Theoretical and experimental analysis of the gating performance of a photocathode-gated image tube using a femtosecond laser

Kan Wu, Xinwan Li,* Chong Shao, and Jianping Chen

Department of Electronic Engineering, Shanghai Jiao Tong University, 800 Dong Chuan Road, Shanghai 200240, China

*Corresponding author: lixinwan@sjtu.edu.cn

Received 4 February 2009; revised 1 May 2009; accepted 26 May 2009; posted 27 May 2009 (Doc. ID 107003); published 10 June 2009

We study theoretically and experimentally the gating performance of photocathode-gated image tube. A cross-correlation method is proposed to analyze the rising and falling speed and width of the image tube gain. Femtosecond pulses generated by a fiber laser are used as the light source of ultrahigh temporal resolution and trapezoid electrical signals are applied to a photocathode electrode as gating pulses. By adjusting the time delay between the laser pulse and the electrical gating pulse, various acceleration procedures for the photoelectrons generated at the photocathode can be observed. The photoelectrons arriving at the multichannel plate (MCP) with different kinetic energies receive different gain according to Eberhardt's MCP gain model. The gain profile is obtained by measuring the output light power of the fluorescent screen at the output port of the tube. The theoretical analysis and experimental result show that the shape of the output gain curve of the image tube is deformed and the width is broadened in comparison with the symmetric electrical gating pulse.

OCIS codes: 100.4550, 110.2970, 120.1880, 320.7100.

1. Introduction

Gated image tubes are widely used to supervise the process of fast phenomena in biological, chemical, and physical reactions. Wang *et al.* proposed a two-dimensional fluorescence lifetime image system with nanosecond time resolution by using a gated image tube for pattern analysis of chemical samples [1,2]. Webb *et al.* developed a similar system with a higher time resolution (~100 ps) to study anatomical features of biological or chemical tissues [3]. Davies *et al.* used a gated image tube to analyze the dynamic instability growth and other plasma phenomena of a magnetized *Z*-pinch [4]. There are two methods to realize the gating ability of image tubes; one is to apply a high-voltage pulse on a microchannel plate (MCP), the other is to apply a high-voltage pulse on photocathode. There have been reports studying the gating performance of MCP gated image tubes. Ito *et al.* studied the time properties of MCP by computer simulation [5]. Failor *et al.* studied MCP gating features and calculated the output gain curve of image tube for Gaussian gating pulse [6]. So far, less attention has been paid to the gating features of photocathode-gated image tubes. In this paper, we study its gating performance theoretically and experimentally. The paper is organized as follows. Analysis of the dynamic process of photoelectrons inside the tube is performed and the gain profile deformations, including broadening and tilting effects, are calculated in Section 2. In Section 3, an experimental system is developed to verify the theory by using femtosecond laser pulses to cross correlate the electrical gating pulses. Section 4 is the discussion of theoretical and experimental results. Section 5 is the conclusion.

0003-6935/09/183337-07$15.00/0

2. Theory

Figure 1 shows the typical structure of the image tubes and the time nodes of the dynamic process when photoelectrons propagate in the image tube. The photocathode is a kind of photoelectrical material. When it is exposed to light (optical signal) the photoelectrons will emit. The photoelectrons, whose spatial distribution corresponds to the image of the input optical signal, are accelerated by the electrical field between the photocathode and the MCP front panel formed by the gating pulse and are multiplied when they pass through the MCP. They are accelerated further by the electrical field between the MCP rear panel and the anode (fluorescent screen) and lighten the fluorescent screen, producing output light.

The dynamic process of the electrons inside the tube can be divided into three subprocesses (phases).

1. Phase I, gating/accelerating subprocess.

At time $t = 0$, an electrical gating pulse is applied onto the photocathode and its front edge forms a time-varied acceleration field between the photocathode and the MCP front panel. At time $t = \Delta t$, a femtosecond laser pulse reaches the photocathode and photoelectrons emit. At time $t = \Delta t + t_{PC}$, photoelectrons reach the front panel of the MCP.

2. Phase II, electron multiplication subprocess.

When the electrons propagate through the microchannels in the MCP, they hit the inside walls of the microchannels and obtain multiplication. The electrical field inside the MCP is constant. The electrons will transit through the MCP in time t_{MCP}.

3. Phase III, imaging to screen subprocess

The electrons obtain acceleration from the constant electrical field between the MCP rear panel and the anode (fluorescent screen) and finally lighten the fluorescent screen in time t_{FS}.

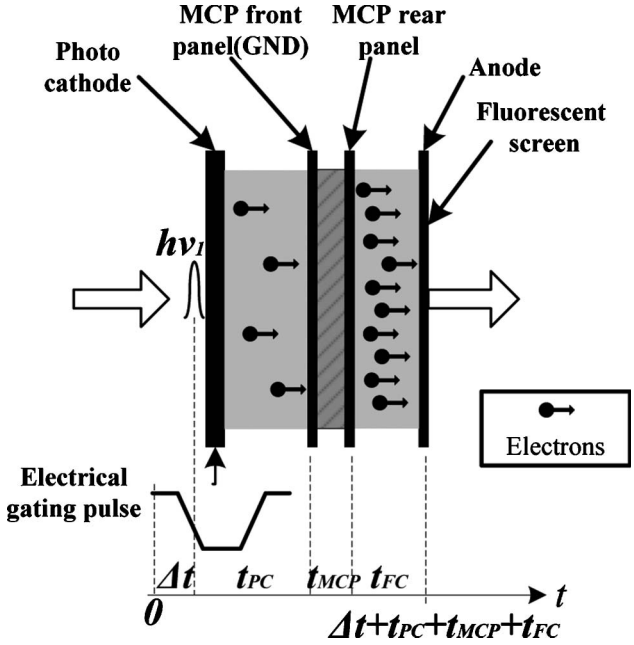

Fig. 1. Typical structure of a photocathode-gated image tube and the process of electrons propagating in the tube.

Based on the above subprocesses, we analyze the basic mechanism of the gating characteristics of photocathode-gated image tubes. As mentioned in phase I, Δt is the time delay of the femtosecond laser pulse with respect to the electrical gating pulse. Photoelectrons generated by laser pulse will obtain different acceleration rates for different Δt. For example, if Δt is small, electrons will be mainly accelerated by the electrical field formed by the front edge of the gating pulse. The acceleration will therefore be small and time varied. If Δt is moderate, the electrons will be accelerated by the field formed by the flat top of gating pulse. The acceleration of electrons will therefore be large and constant. For an excessively long Δt, the electrons will totally miss the acceleration of the gating pulse and will propagate through the distance relying on their original energy at the photocathode. The electrons with different kinetic energies obtain different gains in the MCP in phase II, according to Eberhardt's MCP gain model [7], and this results in different light power outputs at the fluorescent screen in phase III. By adjusting the time delay between the laser pulses and the gating pulses and measuring the related output light power at the fluorescent screen, the gain characteristics of the image tubes can be known.

The purpose of using a femtosecond laser is as follows. The output signal is the cross correlation of the target signal (i.e., gating pulse) and the reference signal (i.e., laser pulse ~100 fs in width). Since the time duration of the reference signal is 4 orders smaller than that of the target electrical gating pulse ~1 ns in width, the femtosecond pulse can be regarded as an ideal impulse with infinite small time duration and the output of cross correlation becomes the exact shape of the target signal.

Another point to mention is that the photoelectrons generated at the photocathode will reach the MCP relying on their original energy even though there is no acceleration electrical field. But the propagation time is relatively long. For example, with the parameters in this paper, this free propagation time is $t_{free} = L/v_0 = \sim 5.7$ ns, where L is the distance between the photocathode and the MCP front panel (2 mm) and v_0 is the initial velocity of photoelectrons (for 780 nm incident light, $v_0 = \sqrt{2E/m_e} = 3.511 \times 10^4$ m/s). So usually a reverse voltage (e.g, +40 V) will be applied to the photocathode to avoid this kind of free propagation. However, when we implemented the gating pulse generator, we found that adding a DC bias voltage might deteriorate the impedance matching between the gating pulse and the photocathode. Therefore, in our experiment the DC reverse bias voltage was removed.

For phase I, Einstein's photoelectric effect equation is used to describe the emission process of the photocathode:

$$h\nu = (1/2)m_e v^2 + h\nu_0, \quad (1)$$

where $h = 6.626 \times 10^{-34}\,\mathrm{m^2kg/s}$ is the Planck constant, $m_e = 9.109 \times 10^{-31}\,\mathrm{kg}$ is the mass of an electron, and ν_0 is the lowest frequency of incident light to help photoelectrons emit from the surface of metal. For multialkali material S25 of the photocathode, the maximum response wavelength is ~1000 nm [8], so $\nu_0 = c/1000\,\mathrm{nm}$, where c is the light speed in vacuum.

As the wavelength of the incident light is known, the kinetic energy of photoelectrons can be calculated. For 780 nm light, the corresponding kinetic energy is 5.61×10^{-21} J or 0.351 eV, which is similar to the result in [7], and the velocity of the photoelectrons is $v_0 = 3.511 \times 10^4\mathrm{m/s}$.

When photoelectrons transit from the photocathode to the MCP front panel, the acceleration of the photoelectrons should be time varied at

$$a = \mathrm{eV}(t)/m_e L, \quad (2)$$

where e is the electron's charge, $V(t)$ is the voltage of the gating pulse, and L is the distance between the photocathode and the MCP front panel. Suppose the time delay between the electrical gating pulses and the femtosecond pulses is Δt and the propagation time of the electrons from the photocathode to the MCP front panel is t_{PC}. The velocity and propagation distance of electrons satisfy the following equations:

$$v(\Delta t + \tau) = v_0 + \int_0^{\tau} a(\Delta t + t)\mathrm{d}t, \quad (3)$$

$$L = \int_0^{t_{\mathrm{PC}}} v(\Delta t + \tau)\mathrm{d}\tau = \int_0^{t_{\mathrm{PC}}} \mathrm{d}\tau \int_0^{\tau} a(\Delta t + t)\mathrm{d}t. \quad (4)$$

By solving the nonlinear Eq. (4) with the numerical arithmetic method, the propagation time $t_{\mathrm{PC}}(\Delta t)$ versus different time delay Δt can be obtained. The input electrical gating pulse is designed close to an ideal trapezoid shape with the same rising and falling time of 0.3 ns and full width at half-maximum (FWHM) of 6 ns, as shown in Fig. 2. The overshoot and ripple in a real electrical pulse are neglected in order to better understand how the propagation time $t_{\mathrm{PC}}(\Delta t)$ is influenced by the rising and falling edges of the electrical pulse. The start time for the gating pulse to be applied is 7 ns. This setting helps to clarify the performance of the photoelectrons during the whole gating period.

The calculated $t_{\mathrm{PC}}(\Delta t)$ is shown in Fig. 2, which can be divided into different regions with respect to Δt. In the region of $\Delta t \le 1.3$ ns, the emitted electrons obtain no acceleration at all and $t_{\mathrm{PC}}(\Delta t) \equiv t_{\mathrm{free}}$, where $t_{\mathrm{free}} = 5.7$ ns. In the region of $1.3\,\mathrm{ns} < \Delta t \le 7\,\mathrm{ns}$, the electrons will partially obtain acceleration and this results in a relatively slowly decreasing curve of propagation time versus time delay. In the region of $7\,\mathrm{ns} < \Delta t \le 13\,\mathrm{ns}$, the electrons will

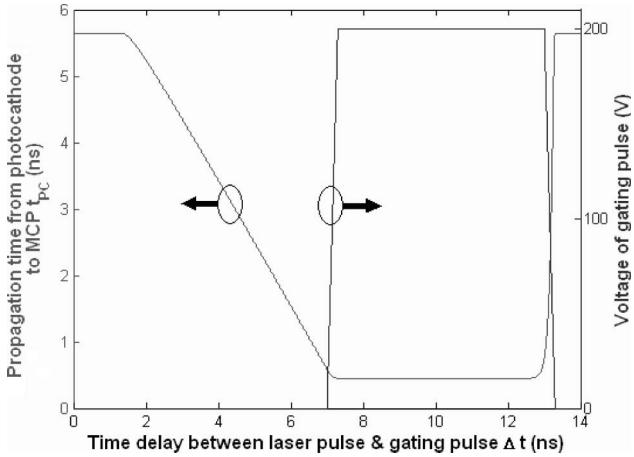

Fig. 2. Waveform of the electrical gating pulse and the propagation time of electrons versus different time delays between laser pulses and electrical gating pulses.

be fully accelerated by the electrical field formed by the flat top of gating pulse and, therefore, propagation time reaches the minimum. In the region of $\Delta t > 13$ ns, the electrical pulse vanishes quickly. As a result, the electrons only obtain very limited acceleration during the propagation and transit through almost the whole distance relying on their original kinetic energy. This forms a sharp rising edge of propagation time t_{PC}. The difference at the rising edge and falling edge of gating pulse will cause the aberration and broadening of the gain curve of the tube, as will be proved in the following parts.

For the behaviors of the electrons in phase II, the equation deduced by Eberhardt can be used to describe the relation between the MCP gain and the incident electron energy in Eq. (5) [7], which is then simplified by using a constant A to represent all constant parameters:

$$\begin{aligned} G &= \delta_1 (V/nV_c)^{k(n-1)} \\ &= \gamma[(nV_{pk} + V)/nV_c]^k (V/nV_c)^{k(n-1)} \\ &= A(nV_{pk} + V)^k, \end{aligned} \quad (5)$$

where n, V_{pk}, V, V_c, and k are the number of dynodes (in this calculation $n = 16$), incident energy of electrons (eV), voltage on the MCP (800 V), the minimum potential for unity secondary emission ratio, and the parameter describing the structural characteristics of the MCP (in this calculation $k = 0.75$), respectively. The normalized gain of the MCP with time delay can be calculated as shown in Fig. 3.

For phase III, the propagation time $t_{\mathrm{MCP}}(\Delta t)$ in the MCP and the time $t_{\mathrm{FS}}(\Delta t)$ from the MCP rear panel to the anode can be calculated simply by the Newtonian motion equation, noting the voltages at the MCP (800 V) and the anode (fluorescent screen, 6000 V) are constant.

According to the above analysis, the propagation process of photoelectrons in the three dynamic phases can be summarized as follows. When the

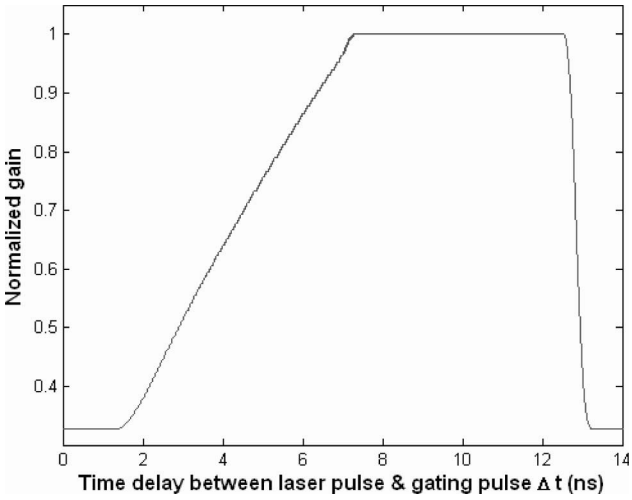

Fig. 3. Normalized gain that the electrons obtain when they pass through the MCP with different incident energy caused by different time delays.

photoelectrons excited by laser pulses emit at time $t = \Delta t$, they will reach the anode (fluorescent screen) and be converted to light at time $t = \Delta t + t_{PC} + t_{MCP} + t_{FS}$ with gain $G(\Delta t)$. Because $G(\Delta t)$ on the MCP gain curve actually represents the output gain at time t, the measured output gain $G_{out}(t)$ at the output of the fluorescent screen can be obtained by using such a time mapping $\Delta t \Rightarrow \Delta t + t_{PC} + t_{MCP} + t_{FS} = t$ as follows: $G(\Delta t) \equiv G_{out}(\Delta t + t_{PC} + t_{MCP} + t_{FS}) \equiv G_{out}(t)$. The normalized output gain curve $G_{out}(t)$ with time mapping is shown in Fig. 4. The gating pulse is 6 ns in width with 300 ps rising and falling edges.

There are two issues to be addressed. One is the change of gain shape as shown in Fig. 4. Compared with the symmetric shape of the electrical gating pulse, the shape of the output gain curve is deformed and broadened. The rising and falling edges of the gain curve are ~0.2 ns and ~0.5 ns, respectively. The FWHM of the gain curve is broadened to 6.3 ns. Further, the falling edge of the gain curve has been elongated in comparison with the steep rising edge. Such an elongating effect is due to the quick increase of the propagation time of electrons in the image tube at the rear edge of the gating pulse.

The second issue is the background noise in the gain diagram in Fig. 4. The existence of background noise can be explained as follows. In order to achieve a better impedance match between the gating pulse and the photocathode electrode, we removed the DC reverse bias voltage, which can prohibit the electrons' free propagation from the photocathode to the MCP. Therefore, even though there is no gating pulse to turn on the image tube, the photoelectrons generated by femtosecond laser pulses will reach the MCP with their original energy and obtain gain in the MCP. These "useless" photoelectrons will finally reach the fluorescent screen of the tube and form the background noise. In Fig. 4, the normalized value of background noise is ~0.33 and the signal-to-noise ratio (SNR) is therefore ~3.

The performance of the output gain curve can be further studied by changing the input gating pulse width. Figure 5 shows the details for input gating pulses with widths of 0.5 ns, 0.8 ns, 1.5 ns, and 4.5 ns. The relation between rising edge, falling edge, and width of the output gain curve and the width of the input gating pulse is shown in Fig. 6. The calculated result shows that the rising edge and the falling edge of gain will not change if the input gating pulse is wide enough (for 300 ps input rising and falling edges, the input width should be greater than 0.8 ns). If the input gating pulse is very narrow (e.g., 0.5 ns), the rising edge and the falling edge of gain will decrease slightly. For $t_{in} > 0.8$ ns, the relation between output gain width, t_{out}, and input gating pulse width, t_{in}, is linear, as in Fig. 6(b), and is given by

$$t_{out} \approx t_{in} + 0.22\,\text{ns}. \quad (6)$$

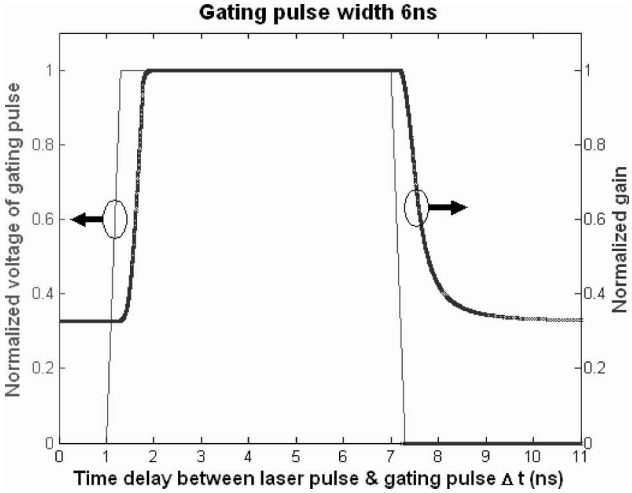

Fig. 4. Normalized output gain curve versus time when considering all three subprocesses of the electrons in the gated image tube.

3. Experiment

The schematic layout of the experimental system is shown in Fig. 7. The output pulse width of the femtosecond laser is ~100 fs centered at 780 nm and the repetition rate is 40 MHz (fiber laser FFL-780 by Precision Photonics Corporation). The output power of the laser is ~10 mW. The power meter used is a lightwave multimeter with power meter card HP81533A and detection head HP81520A.

For the optical route (dashed line in Fig. 7), a movable mirror and a 50:50 beam splitter (BS1) are used to delay the laser pulses precisely and the second 50:50 beam splitter (BS2) is used to provide a signal for the photodetector to synchronize with the electrical gating pulse. BS1 and BS2 attenuate the light power by 9 dB (6 dB by BS1, 3 dB by BS2) to limit the light power to an appropriate level for the photodetector.

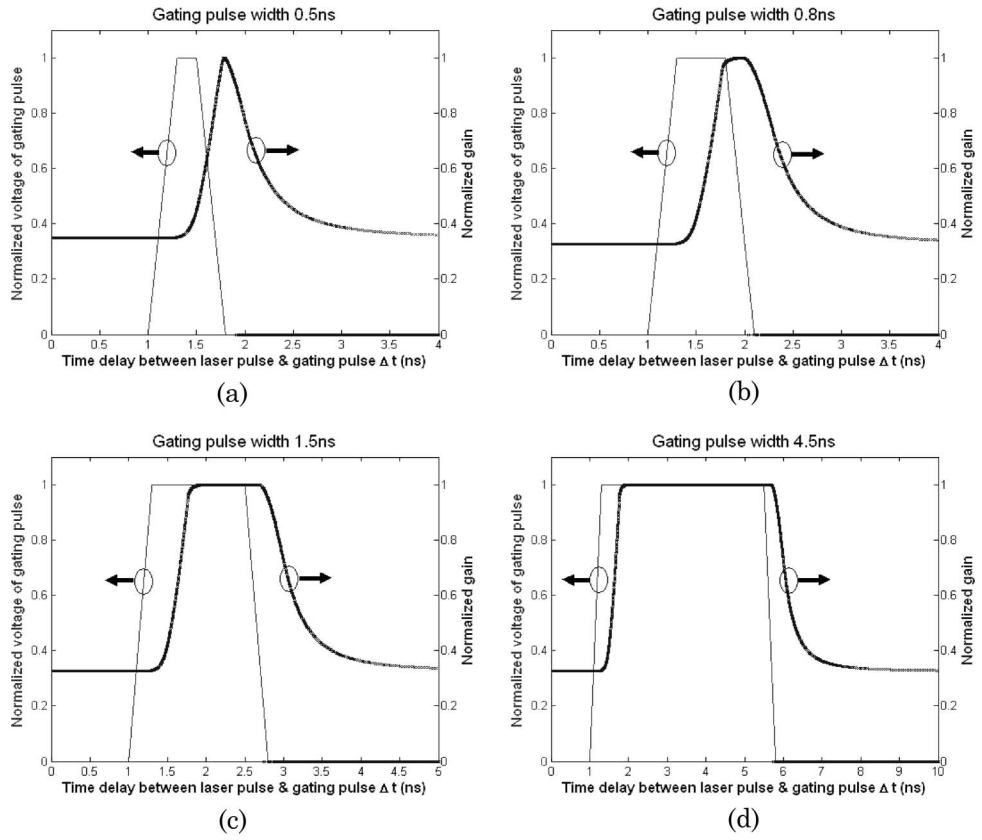

Fig. 5. Normalized gain curve of the image tube versus different input widths of gating pulses: (a) 0.5 ns, (b) 0.8 ns, (c) 1.5 ns, and (d) 4.5 ns.

For the electrical route (solid line in Fig. 7), the synchronous output of the laser is generated by an internal photo detector. It passes through a pulse reshaper and amplifier to meet the requirement of the following 3.3 V digital circuits. A 40 MHz repetition rate of laser pulses is too high for the fluorescent screen, which has a relaxation time of a few milliseconds, so the shaped synchronous signal passes through a frequency divider to reduce the repetition rate from 40 MHz to 10 Hz. A delay device has been inserted to generate time delay: 200 ps, 400 ps… 25.6 ns, which can be regarded as a coarse delay and the set including the moving mirror and BS1 is used to generate a precision delay. With the cooperation of these two parts, laser pulses can scan the whole time duration of the electrical gating pulse. Since the width of the electrical pulse is about 6.1 ns, shown in Fig. 8(a), and the interval between two adjacent laser pulses is about 25 ns, only one laser pulse will "see" the electrical gating pulse and the

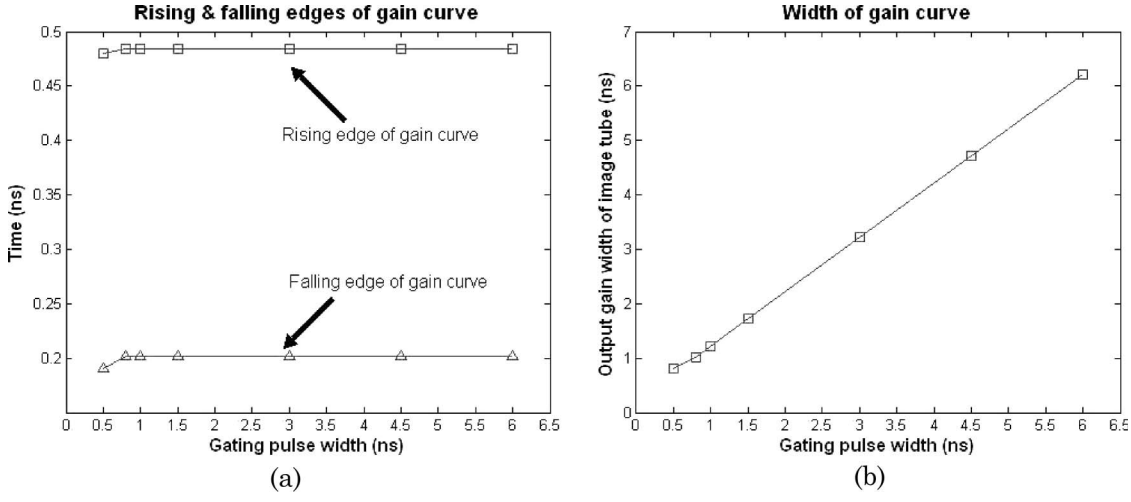

Fig. 6. Rising and falling edges and the width of the output gain of the image tube for different input widths of the gating pulse.

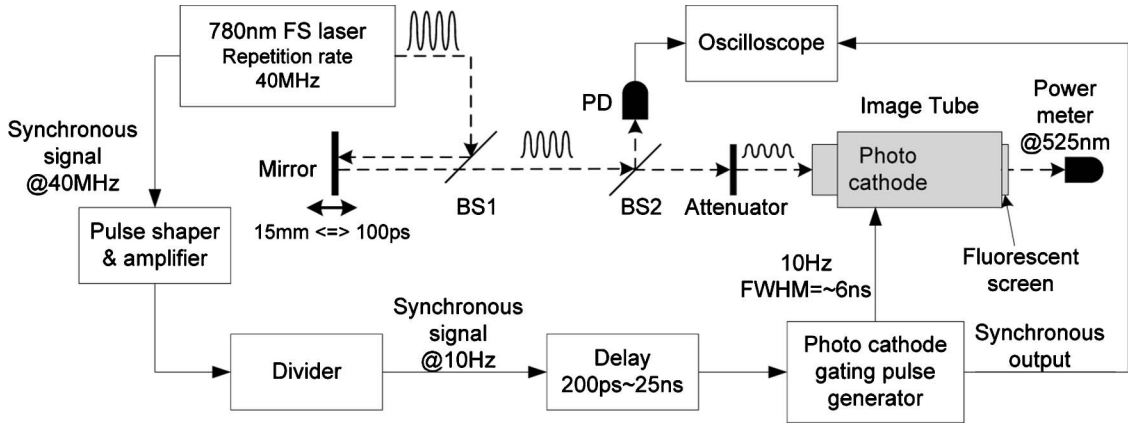

Fig. 7. Schematic layout of the measurement of the gating response in the photocathode-gated image tube.

rest of the laser pulses will not work during the measurement until the next gating pulse comes.

The measured light power output by the image tube is shown in Fig. 8(b). This power is only a small portion of its real value due to the low coupling efficiency. The resolution of the power meter is 10 pW, which is much smaller than the measured data. The time step of scanning is 200 ps. The timing jitter of the electrical route is less than 100 ps. The gain region is approximately 6.4 ns (FWHM) which is close to the theoretical estimation. The average power at the gain region is ~31.5 nW and the average power of background noise is ~17.5 nW. The SNR is $31.5/17.5 = \sim 1.8$, which is smaller than the estimation. The ripple of background noise in Fig. 8(b) might be caused by the ripple after the trailing edge of the gating pulse in Fig. 8(a). The output gain width of the image tube versus the different width of the input gating pulses was also measured, as shown in Fig. 9. The measured data fit the theoretical estimation well.

4. Discussion

There are some issues to be discussed. The first is about the noise. The noise mainly consists of following five factors: intrinsic noise of the proposed cross-correlation method, intrinsic noise of the image tube, noise fluctuation of the image tube, noise induced by the fluctuation of the gating pulse, and noise induced by timing jitter. The formation of intrinsic noise of our measurement method has been explained in the end of Section 2. In Fig. 8(b), this noise is ~17.5 nW. The intrinsic noise and the noise fluctuation of the image tube are ~30 pW and can be neglected. These three kinds of noise form the theoretical background noise of the output gain curve. The noise induced by fluctuation of the gating pulse and timing jitter cause the fluctuation of the gain curve in the actual experiment. Since the proposed cross-correlation method requires an integral process in the time domain, the fluctuation of the voltage of the gating pulse will cause the fluctuation of the gain curve. Timing jitter will also cause the fluctuation of the gain curve. The noise induced by the gating pulse and timing jitter is ~4 nW in Fig. 8(b).

The second issue is about the decrease of the SNR. The experimental result of the SNR is ~1.8 as measured in Section 3, which is smaller than the theoretical SNR (~3) as estimated in Section 2. The

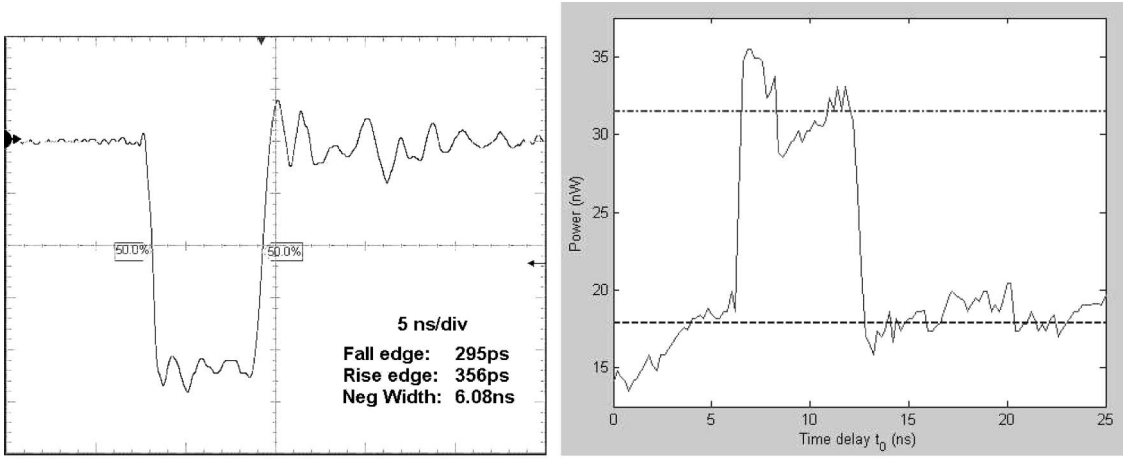

(a) (b)

Fig. 8. (a) Input gating pulse and (b) measured output light power at the fluorescent screen. Dashed-dotted line is the average power at the gain region and the dashed line is the average power of background noise.

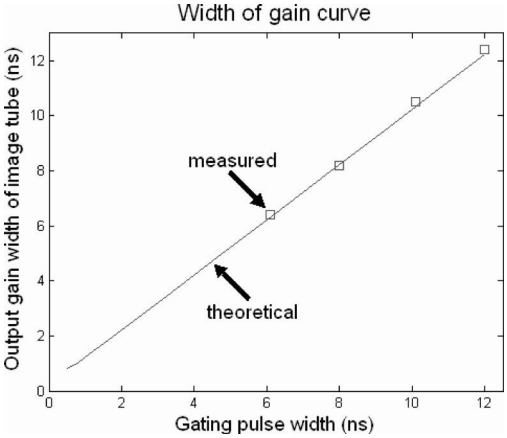

Fig. 9. Measured output gain width of the image tube versus different widths of input gating pulses.

decrease of the SNR is probably caused by two reasons: the first is the mismatch of the repetition rate between the two correlated signals. The repetition rate of laser pulses (40 MHz) is higher than that of the electrical gating pulse (10 Hz). The photoelectrons generated by these "needless" laser pulses still obtain gain according to the gain curve in Fig. 4 and, therefore, the background noise has been lifted. The second reason is nonlinearity of fluorescent efficiency of the screen. The efficiency of electrical photoconversion of the fluorescent screen is dependent on the energy of the electrons hitting it. However, it is difficult to measure with the devices available in our lab. It will help determine which aspect is the main reason for the decrease of the SNR to use a high-speed Pockel cell or an acousto-optic modulator to directly reduce the repetition rate of the laser pulses.

The last issue to be discussed is the difference between the theoretical gain curve in Fig. 4 and the real measured output curve in Fig. 8. The rising and falling edges of the theoretical gain curve are ~0.2 ns and ~0.5 ns, while the measured rising and falling edges of the output curve in Fig. 8 are ~300 and ~600 ps, respectively. The FWHM of the theoretical gain curve is 6.3 ns while the measured FWHM of the output curve in Fig. 8 is 6.4 ns. These differences are due to the existence of overshoot and ripple in the practical gating pulse, which is different from the ideal trapezoid shape of the gating pulse for simulation. The vibration in the gain region (approximately 6–13 ns) in Fig. 8(b) is due to the plank capacitance structure of the image tube which resulted in the impedance mismatch between the electrical gating pulse (designed for 50 ohm resistance load) and the photocathode electrode (capacitance load).

5. Conclusions

In this paper, the dynamic process is analyzed when the electrical gating pulse is used to turn on the photocathode-gated image tube and the theoretical calculation is verified by using a femtosecond laser to cross correlate the electrical gating pulses.

The theoretical analysis shows that, when a symmetric input gating pulse is applied to the image tube, the output optical gain curve will be a deformed curve and the width will be broadened in comparison with the width of the input gating pulse. The rising and falling edges of the gain curve are independent on the gating pulse width when it is wide enough (e.g., >1.5 ns). For a narrow gating pulse (e.g., <800 ps), however, the rising and falling edges of the gain curve will be slightly affected by the gating pulse width. The experimental verification also shows that the measured width of the gain curve has broadened to 6.4 ns in comparison with the input electrical gating pulse (6.1 ns in width). The falling edge of 600 ps and the rising edge of 300 ps of the gain curve indicates that a deforming effect happens during the gating process.

The theoretical analysis and experiment exhibit that the proposed cross-correlation method is effective to study the gating performance of the image tube. It will be helpful for researchers to use the image tube properly. For example, the broadening of the gain curve will lead to the distortion of the image. The shape of the gating pulse should be carefully set for specific applications.

The authors appreciate the enlightening discussion with Dinghuan Deng, Shuguang Li, and Wei Dai during the experimental setup. This work was supported in part by the National Science Foundation of China (NSFC) (90704002, 60877012), 863 Project (2006AA01Z242 and 2007AA01Z275), Dawn Program for Excellent Scholars by the Shanghai Municipal Education Commission (06SG15), and the Key Disciplinary Development Program of Shanghai (T0102).

References

1. X. F. Wang, T. Uchida, D. M. Coleman, and S. Minami, "A two-dimensional fluorescence lifetime imaging system using a gated image intensifier," Appl. Spectrosc. **45**, 360–366 (1991).
2. X. F. Wang, T. Uchida, M. Maeshima, and S. Minami, "Fluorescence pattern analysis based on the time-resolved ratio method," Appl. Spectrosc. **45**, 560–565 (1991).
3. S. E. D. Webb, Y. Gu, S. Leveque-Fort, J. Siegel, M. J. Cole, K. Dowling, R. Jones, and P. M. W. French, "A wide-field time-domain fluorescence lifetime imaging microscope with optical sectioning," Rev. Sci. Instrum. **73**, 1898–1907 (2002).
4. H. M. Davies, A. E. Dangor, M. Coppins, and M. G. Haines, "Measurement of instability growth in a magnetized *Z* pinch in the finite-Larmor-radius regime," Phys. Rev. Lett. **87**, 145004 (2001).
5. M. Ito, H. Kume, and K. Oba, "Computer analysis of the timing properties in micro channel plate photomultiplier tubes," IEEE Trans. Nucl. Sci. **31**, 408–412 (1984).
6. B. H. Failor, D. F. Gorzen, C. J. Armentrout, and G. E. Busch, "Characterization of two-gated microchannel plate framing cameras," Rev. Sci. Instrum. **62**, 2862–2870 (1991).
7. E. H. Eberhardt, "Gain model for microchannel plates," Appl. Opt. **18**, 1418–1423 (1979).
8. L. Liu and B. Chang, "Spectral matching factors between super S25 and new S25 photo cathodes and reflective radiation of objects," Appl. Opt. **43**, 616–619 (2004).